AIMS Materials Science, 9(1): 71–84.
DOI: 10.3934/matersci.2022005
Received: 08 October 2021
Revised: 11 November 2021
Accepted: 15 November 2021
Published: 29 December 2021

http://www.aimspress.com/journal/Materials

Research article

Exchange bias, and coercivity investigations in hematite nanoparticles

Venkatesha Narayanaswamy[1], Imaddin A. Al-Omari[2], Aleksandr. S. Kamzin[3], Chandu V. V. Muralee Gopi[4], Abbas Khaleel[5], Sulaiman Alaabed[6], Bashar Issa[1,*] and Ihab M. Obaidat[7,*]

[1] Department of Medical Diagnostic Imaging, College of Health Sciences, University of Sharjah, Sharjah, P.O. Box 27272, UAE
[2] Department of Physics, Sultan Qaboos University, P.O. Box 36, Muscat PC 123, Sultanate of Oman
[3] Ioffe Physical Technical Institute, St. Petersburg, 194021, Russia
[4] Department of Electrical Engineering, University of Sharjah, Sharjah, P.O. Box 27272, UAE
[5] Department of Chemistry, United Arab Emirates University, Al-Ain 15551, UAE
[6] Department of Geology, United Arab Emirates University, Al-Ain 15551, UAE
[7] Department of Physics, United Arab Emirates University, Al-Ain 15551, UAE

* **Correspondence:** Email: iobaidat@uaeu.ac.ae, bissa@sharjah.ac.ae; Tel: +971-3-713-6321.

Abstract: Hematite nanoparticles of average size of 20 nm were synthesized using sol-gel method and the structural characterisations were conducted using XRD and TEM. The XRD profile revealed the coexistence of small fraction of maghemite phase along with the main hematite phase. Magnetization versus applied field (M-H) measurements were performed between −5 and 5 T and respectively in the temperatures 2, 10, 30, 50, 70, 100, 150, 200, and 300 K under zero field and 1, 2, 3, 4 T field cooling. At all field-cooling values, the coercivity was found to display a weak temperatures dependence below 150 K and a strong increase above 150 K reaching the largest value of 3352 Oe at 300 K for the field-cooling value of 3 T. Horizontal and vertical hysteresis loop shifts were observed at all temperatures in both the zero-field and field-cooled states. In the field-cooled state, both loop shifts where found to have significant and nonmonotonic field-cooling dependences. However, because saturation magnetization was not attained in all measurements our calculations were based on the minor hysteresis loops. M-H measurements were performed between −9 and 9 T at room temperature under zero field cooling and 1, 2, 3, 4, 5, 6 T field cooling. Saturation magnetization was not attained, and the loops displayed loop shifts similar to those for the ±5 T sweeping field. The highest coercivity

value of 4400 Oe is observed for the 6 T field cooled MH loop. The ferromagnetic (FM) contribution towards the total magnetization was separated from the total magnetization and hysteresis loops displayed both horizontal and vertical shifts. The novel results of the temperature and field dependence of exchange bias were attributed mainly to the magnetic exchange coupling between the different magnetic phases (mainly the FM) and the spin-glass-like regions.

Keywords: nanoparticles; hematite; exchange bias; coercivity; Morin transition; surface spins

1. Introduction

In recent years, the nanoparticles have attracted the researcher's interest and have been extensively studied due to their diverse applications in biotechnology, environment protection, data storage, magnetic sensor, and drug delivery [1–5]. The nanoparticles' properties depend on the size, shape, morphology, crystallinity, surface effects, and inter-particle interactions of the materials [6,7]. Hence, understanding the fundamental properties of the nanomaterials is the prerequisite for their widespread applications. Iron oxide nanoparticles have drawn remarkable attention in biomedical applications such as MRI (as contrast agents) and magnetic hyperthermia [8,9]. Iron oxide exists mainly in the form of maghemite, magnetite and hematite. Maghemite and magnetite forms a spinel cubic structure, where Fe spins are distributed in tetrahedral and octahedral sites, which are magnetically coupled through double exchange. Both phases are ferrimagnetic in nature due to the opposite spins of A (tetrahedral) and B (octahedral) sites [10]. The magnetic properties of these particles are highly size dependent where below certain critical sizes the nanoparticles of both maghemite and magnetite possess superparamagnetic nature at room temperature. This property enables them to use in biomedical applications as they respond to external magnetic field and aggregation is avoided upon removal of external magnetic field [11].

The hematite is the most stable oxide of iron, which is commonly found in rocks and soil naturally. Because of its stability and low cost of mining hematite is most studied natural material for catalytic, gas sensor, electrochemical, inorganic pigments, and water purification applications [12,13]. Hematite is synthesised by various chemical and physical methods. Liu et al. was able to synthesize quasi, irregular cubic, parallel hexahedron sphere, nanosheet and hexagon shaped α-Fe_2O_3 structures using anions surfactants like OH^-, Cl^-, SO_4^{2-}, NO^{3-} and CH_3COOH. They have shown that the magnetic and optical properties of α-Fe_2O_3 nanoparticles have a significant dependency on the shape of the nanoparticles [14]. The physical method of synthesis like ball mill results in a more active surface spin configuration of nanoparticles, which are evident through their magnetic properties [15].

Hematite (α-Fe_2O_3) exhibits antiferromagnetism and weak ferromagnetism behaviors below and the above the Morin temperature, respectively. Its crystal structure consists of hexagonal close-packed oxygen-sheets with two-third of octahedral interstices between the sheets filled with Fe^{3+}. In antiferromagnetic crystalline (rhombohedral) hematite (α-Fe_2O_3), a spin-reorientation phenomenon (magnetic phase transition called the Morin transition) occurs at $T_M \approx 263$ K [16]. The Morin transition occurs due to the competition between the two different anisotropies with a comparable magnitude but

with opposite signs. Below T_M, the orientation of the two magnetic sublattices are directed toward the rhombohedral axis [111] and exactly antiparallel, and the material is an antiferromagnet. Above T_M, due to the super-exchange interaction, the moments are in the basal plane (111) with slight canting from the antiferromagnetic axis [17]. This causes a small net magnetization, and thus the material becomes weakly ferromagnetic. The Morin transition temperature decreases with decreasing the particle size and tends to zero for the particles with size 10–20 nm or less [18–21]. Surface effects have a significant role in determining the T_M value. α-Fe_2O_3 nanoparticles show superparamagnetic, weak-ferromagnetic, and antiferromagnetic behavior at different stages, and so, α-Fe_2O_3 nanoparticles are exciting materials for the fundamental research [20].

We have reported Morin transition for the α-Fe_2O_3 nanoparticles with respect to various cooling fields in temperature dependent magnetisation experiments. It was found that the Morin transition temperature is slightly field dependent, and it occurred around 250 K [22]. The extent of the transition was broad, and it was attributed to the wide distribution of sizes. The particles also possessed non-zero magnetisation in the antiferromagnetic state and significant magnetisation at room temperature. Attaining considerable ferromagnetic nature for hematite nanoparticles at room temperature is of paramount importance for the potential applications. The exchange bias is obtained by measuring the shift in the M-H (magnetisation versus applied magnetic field) hysteresis loop along the horizontal and vertical direction. Exchange bias is important property of the magnetic nanoparticles, which is required to be investigated, specifically to understand the origin of magnetism due to surface spins and interaction between the magnetic core and surface spins [23]. The hysteresis loop shift causes change in the H_C (coercive field) when the ferromagnetic and antiferromagnetic systems are cooled in a magnetic field. Though the exchange bias effect were reported long back where various systems of magnetic interfaces were subjected to intense studies, the EB phenomena is not completely understood. The origin of EB is attributed to the exchange coupling between FM and AFM moments at the interfaces, which depends on the anisotropy energy. Here we report the temperature and field dependent EB of hematite nanoparticles with small maghemite phase fraction. It is observed that there is significant exchange bias on horizontal direction whereas the exchange bias on vertical direction is negligible.

The magnetisation vs applied magnetic field (M-H) plots were obtained at several temperatures in the field range of −5 to 5 T. The particles were cooled to the required temperatures in zero field and under field values of 1, 2, 3, and 4 T. The shift in the M-H hysteresis loop was used to obtain the exchange bias field. We have investigated the EB dependency on the temperature and applied cooling field in the hematite nanoparticles. The results presented in this study will help in understanding the origin of the exchange bias and in enhancing the room temperature magnetic properties of hematite nanoparticles. We have indicated ferrimagnetic (Maghemite) phase as ferromagnetic because of the similar response to the magnetic field.

2. Materials and methods

2.1. Synthesis

Materials used in the synthesis are iron (III) nitrate nonahydrate at a rate of 98%, titanium (IV) n-butoxide (97%), 2-porpanol (99.7%), and propylene oxide (99%). All chemicals were obtained from Sigma Aldrich and were used as received. Hematite (α-Fe_2O_3) nanoparticles were synthesized by dissolving $Fe(NO_3)_3 \cdot 9H_2O$ salt in 2-propanol solvent and propylene oxide promotor which acts as condensing agent. In the synthesis method 10.7 g of iron salt was dissolved in 100 mL of 2-propanol and 25 mL propylene oxide mixture under constant stirring for 4 h. Upon continues stirring the solution turns into reddish-brown colloidal and it is further aged for 24 h followed by evaporation of the solvent at 80 ℃ in water bath. The brown precipitate is further washed with water and dried for 1 h at 120 ℃. Finally, the solid obtained is calcined at 350 and 500 ℃ for 1 and 4 h respectively.

2.2. Structural characterization

The structure and morphology of the nanoparticles was determined by X-ray diffraction (XRD) and transmission electron microscopy (TEM) images. XRD characterization was carried out using a Shimadzu-6100 powder XRD diffractometer with Cu–Ka radiation with wavelength 1.542 Å. Diffraction data was obtained in an angle range of 20–80 deg with 1 deg/min scan rate. TEM images were obtained using the Philips electron microscope of CM10. The average crystalline size is calculated using Scherrer formula from the full width half maximum (FWHM) of highest intensity peak (110).

2.3. Magnetic measurements

The dc magnetic measurements were carried out using a VSM in Physical Properties Measurement System (PPMS) from Quantum Design. The magnetization versus applied magnetic field (M-H) hysteresis loops were obtained both in the zero-field-cooled (ZFC) and field-cooled (FC) states. For the FC measurements, magnetic field values (H_{FC}) of 1, 2, 3, 4 T field were applied while cooling the particles to the required temperature. All FC M-H loops were recorded in the field range of −5 to 5 T. The particles were cooled down from room temperature to 2, 30, 50, 70, 100, 150, 200, and 300 K before obtaining each M-H plot at that particular temperature. From the M-H plots, we obtained the effect of temperature and H_{FC} values on the horizontal and vertical shifts in the hysteresis loop. The shift in the field values is obtained with the uncertainty of ±1 Oe whereas the error associated with the magnetisation value obtained from the MH plot is ±0.0001 emu/g.

3. Results and discussion

The XRD profile obtained from the sol-gel-synthesized hematite nanoparticles is shown in Figure 1. The diffraction pattern consists of peaks corresponding to α-Fe_2O_3 and small fraction of maghemite phase. Though it indicates the formation of mixed phase, the fraction of maghemite is low,

which is evident from the intensity ratio of maghemite and hematite peaks. Using POWDER-CELL, the unit cell parameters were determined. The lattice dimensions are a = 5.0339 Å and c = 13.7866 Å with a cell volume of 302.5545 $(Å)^3$. The XRD pattern obtained is in agreement with the expected XRD profile of α-Fe_2O_3 phase. By using FWHM of the highest intensity peak (110) corresponding to the α-Fe_2O_3 phase, the average crystallite size of the nanoparticles was obtained. From the XRD profile and using Scherrer formula, the mean diameter of the nanoparticles was calculated to be about 20 nm. The nanoparticles bright field TEM image is shown in Figure 2. The nanoparticles have a twisted spherical appearance and are broadly distributed in size. The size distribution histogram is obtained by measuring the individual nanoparticles sizes using sigma scan software and histogram is shown in Figure 2a, the average sizes of the nanoparticles is 17 nm and the size distribution is broad with significant number of particles having sizes of 11–13 nm.

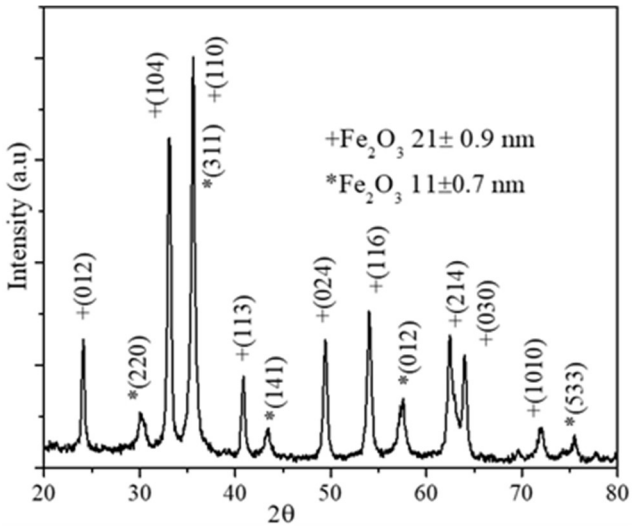

Figure 1. X-ray diffraction pattern of hematite nanoparticles (reprinted with permission from [22]).

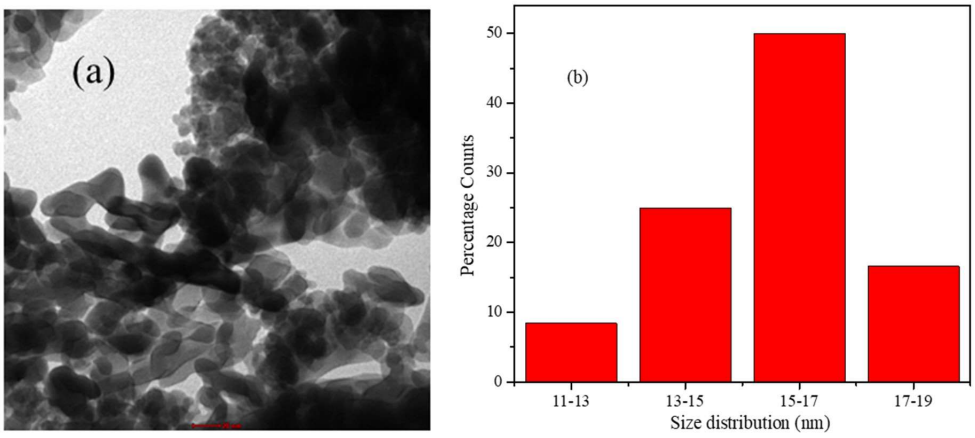

Figure 2. (a) TEM bright field images of hematite nanoparticles illustrating the characteristic particle morphologies. (b) Size distributions of the nanoparticles.

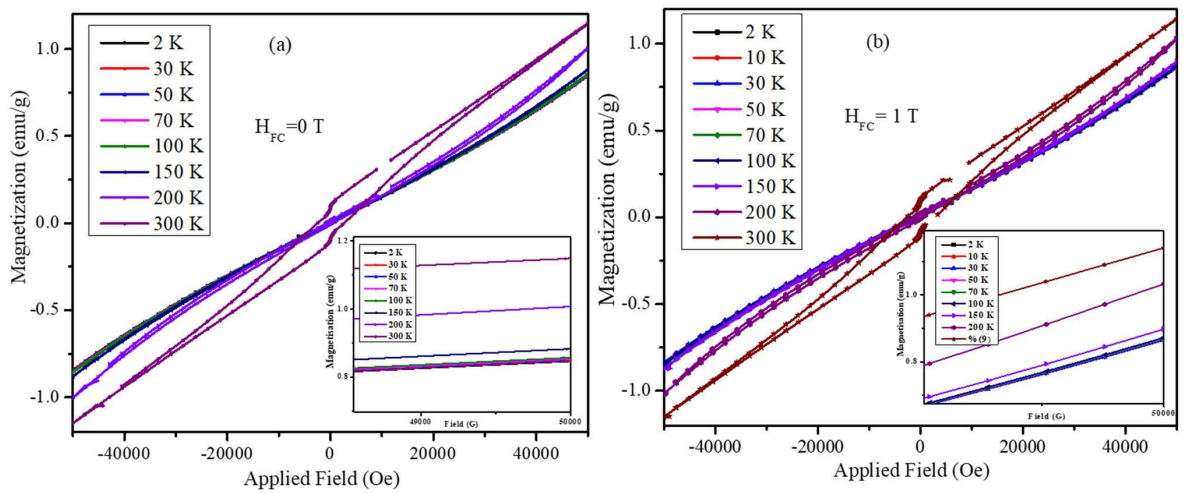

Figure 3. Magnetisation versus the applied magnetic field (M-H) plots at several temperatures (a) In the ZFC state; (b) In the FC state at field cooling value of 1 T.

Figure 3 displays the M-H hysteresis loops for hematite nanoparticles obtained at difference temperatures in the ZFC state and in the FC state at H_{FC} = 1 T. Other M-H plots at various temperatures were obtained at H_{FC} = 2, 3, and 4 T. For each hysteresis loop, the magnetization was measured by varying the magnetic field from −5 to 5 T.

For each hysteresis loop, the temperature was brought to 300 K and then cooled down to the particular temperature in zero applied magnetic field of under a specific H_{FC} value. The hysteresis curve obtained at 300 K shows a loop indicating the ferromagnetic nature of the hematite nanoparticles, which is expected above the Morin transition temperature 250 K. The M-H loops obtained in the temperature range of 2 to 200 K display negligible hysteresis. Although below Morin transition temperature the hematite nanoparticles are expected to have zero magnetization, the observed negligible hysteresis behaviour is attributed to the small fraction of the maghemite phase. Similar paramagnetic behaviour of the hysteresis loops was observed at other cooling fields at temperatures below 200 K. The M-H plots were used to determine the horizontal and vertical exchange bias.

In the previous work [22], at several applied fields these hematite nanoparticles were conducted on zero-field-cooled (ZFC) and field-cooled (FC) temperature dependent magnetisation (M-T) measurements. Morin transition temperature was determined by calculating the first order derivative of magnetisation with respect to temperature (dM/dT). The Morin transition was found to occur at around 250 K. Morin transition showed a slight dependency on the applied magnetic field.

To determine the exchange bias, the shift in the M-H hysteresis loop from the origin was obtained. The enlarged M-H plots at the origin of the hysteresis loops are shown in Figure 4. As evident from the Figure 4, the shift in the hysteresis loops depend on both the field-cooling value and the temperature. The coercivity and exchange bias fields were calculated from the M-H hysteresis loops. The coercivity (or coercivity field, H_C) is defined as the magnetic field value at which the magnetization becomes zero during M-H measurements. It is calculated using the Eq 1:

$$H_C = \frac{|H_{C1} - H_{C2}|}{2} \quad (1)$$

The exchange bias field (H_{EB}) is obtained by the horizontal shift in the hysteresis loops, H_{EB}. The exchange bias field, H_{EB} was calculated using the following formula:

$$H_{EB} = \frac{|H_{C1} + H_{C2}|}{2} \quad (2)$$

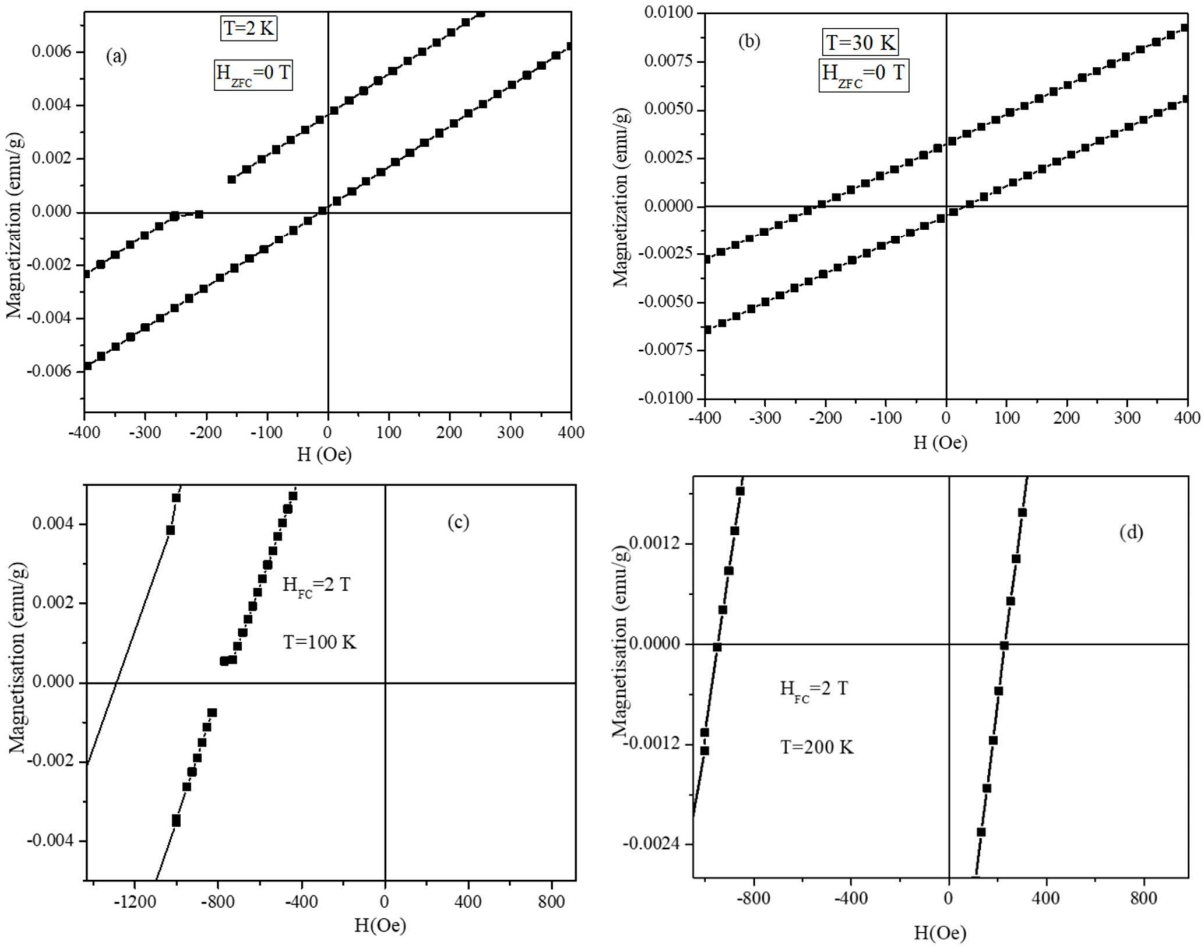

Figure 4. The enlarged M-H plots around the center of the loops (a) in the ZFC state at 2 K, (b) in the ZFC state at 30 K, (c) in the FC state at HFC = 2 T at 100 K, and (d) in the FC state HFC = 2 T at 200 K.

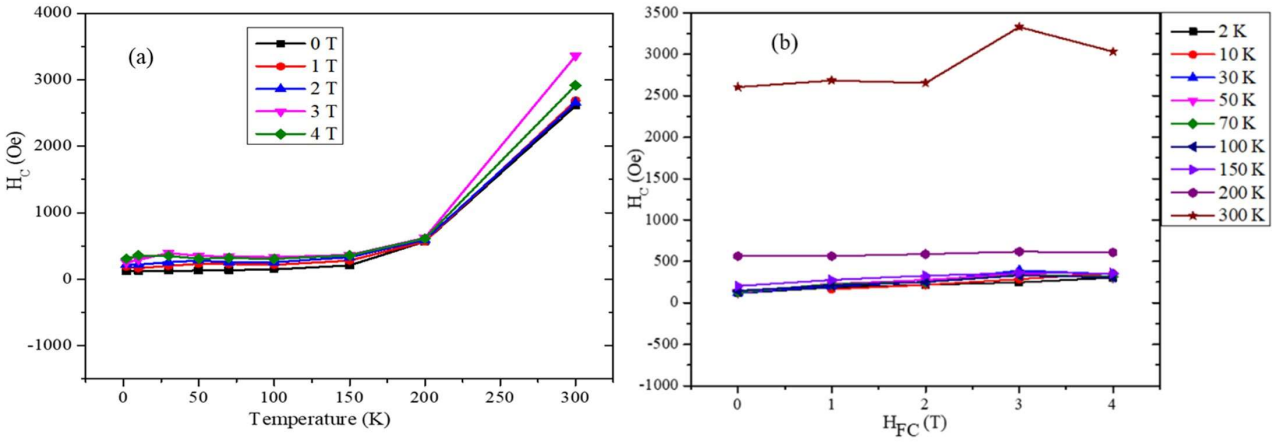

Figure 5. The coercivity in the ZFC state and in the FC state (a) as function of temperature at field cooling values of 1, 2, 3, 4 T, and (b) as function of field cooling at temperatures ranging from 2–300 K.

The coercivity of the hematite nanoparticles was calculated by Eq 1. And the temperature-dependent coercivity plots are shown in Figure 5a where it can be seen that all curves display a similar behaviour. In both the ZFC state and FC state at all H_{FC} values, the coercivity remains constant until 150 K and then increases slightly at 200 K followed by a sharp increase with the increase of temperature. As seen in Figure 5b, large coercivity values are obtained at room temperature (300 K), because of the ferromagnetic nature of the particles, which is induced by the relaxation of basal plane spins along the c-axis. Except at 200 K (where the coercivity is similar for all temperatures and H_{FC} values), the coercivity in the ZFC state is always smaller than that in the FC state.

It can be seen in Figure 5b that there is a peak in coercivity at H_{FC} = 3 T at nearly all temperatures. The peak is more pronounced at 300 K with H_C value of 3352 Oe.

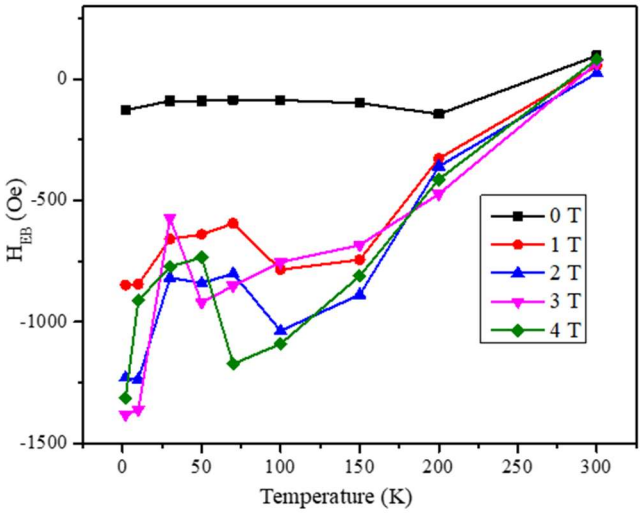

Figure 6. The exchange bias field as a function of temperature in the zero-field-cooled state and in the field-cooled state at field cooling values of 1, 2, 3, 4 T.

Figure 6 displays the exchange bias field (H_{EB}) as function of temperature in the ZFC state and in the FC state at 1, 2, 3, 4 T field-cooling (H_{FC}) values. From the temperature-dependent plots, it can be seen that H_{EB} is negative in both the ZFC and the FC states at all H_{FC} values up to 200 K and is positive at room temperature (300 K). H_{EB} shows a non-monotonic behavior with the temperature under all H_{FC} condition. H_{EB} increases from 2–30 K and drops until 100 K.

It increases slightly above 100 K and increases sharply after 150 K, eventually becomes positive at 300 K. H_{EB} has values of −1365 Oe at 2 K and 90 Oe at 300 K in the ZFC state. H_{EB} remains constant up to 200 K with a value of −102 Oe and is positive at 300 K. At all temperatures, the H_{EB} in the ZFC state is higher than that in the FC state.

The hematite nanoparticles possess significant ferromagnetism at room temperature, which is evident from the observed M-H loops. However, the significant M-H loop opening above the Morin transition temperature could be attributed to the exchange coupling of the (AFM) hematite and the (FM) maghemite phases with the spin-glass (SG) regions at the particle surfaces. The paramagnetic nature of the M-H plots (Figure 3) below 200 K can be attributed to the existence of a small fraction of maghemite phase, and a very slight (about 5%) nonmagnetic phase, which were confirmed by the XRD measurements.

The temperature dependence of the exchange bias in our sample is similar to those reported in iron oxide core-shell nanoparticles and in layered structures which include spin-glass phase [24,25]. Broken bonds and lattice distortions at the surface affect the coordination of surface cations leading to changes in their spin-orbit energy, and thus producing changes in the local magneto crystalline anisotropy [26,27]. Surface spin canting was suggested to occur due to the significant contribution to local magnetism caused by the low symmetry near the surface of the nanoparticles [28]. Hence, we suggest that surface spin freeze in random orientations and form spin glass (SG) clusters at the surface of the nanoparticles. The observed nonmonotonic temperature and field-cooling dependence exchange bias in our sample could be attributed to the exchange coupling between the AFM hematite and the FM maghemite nanoparticles mediated by a SG like phase. The surface SG phase prevents the direct exchange coupling between the nanoparticles. This SG phase is suggested to be composed of canted spins at the surfaces of both types of nanoparticles. These canted surface spins are oriented randomly with variable pinning strengths resulting in a nonmonotonic temperature and field behavior of the exchange bias.

It is very important to clarify two main points here. First, it was reported that exchange bias occurred in various combinations between ferromagnetic (FM), antiferromagnetic (AFM), canted AFM, ferrimagnetic (FIM), and spin glass (SG) magnetic phases [23,29–32]. It is very important to realize that we do not talk about direct FM/AFM exchange bias in our sample. We clearly emphasized that the nonmonotonic temperature and field dependent exchange bias is an indication of magnetic/Spin glass (SG) exchange coupling. In magnetic/SG systems, the exchange bias occurs when cooling through the transition temperature of the magnetic phase (T_C, T_N) or when cooling through the spin glass freezing temperature (T_{SG}) [33,34]. In our system, we have seen direct signs of such spin glass signature in the ZFC/FC magnetization versus temperature measurements reported recently [22] where T_{SG} is below 200 K. Hence, cooling down from 300 K is sufficient for the exchange bias to take place in our samples.

Second, it is correct that the magnetization hysteresis loops were not saturated (minor loops). We have conducted additional hysteresis measurement at room temperature where the field was swapped between ±9 T under zero field and several field-cooling values (1, 2, 3, 4, 5, 6 T) and magnetization did not attain saturation as shown in Figure 7 (for the zero-field cooled and the 2 T-field-cooled state). The loops displayed small loop shifts of similar magnitudes to those obtained with the swapped field between ±5 T.

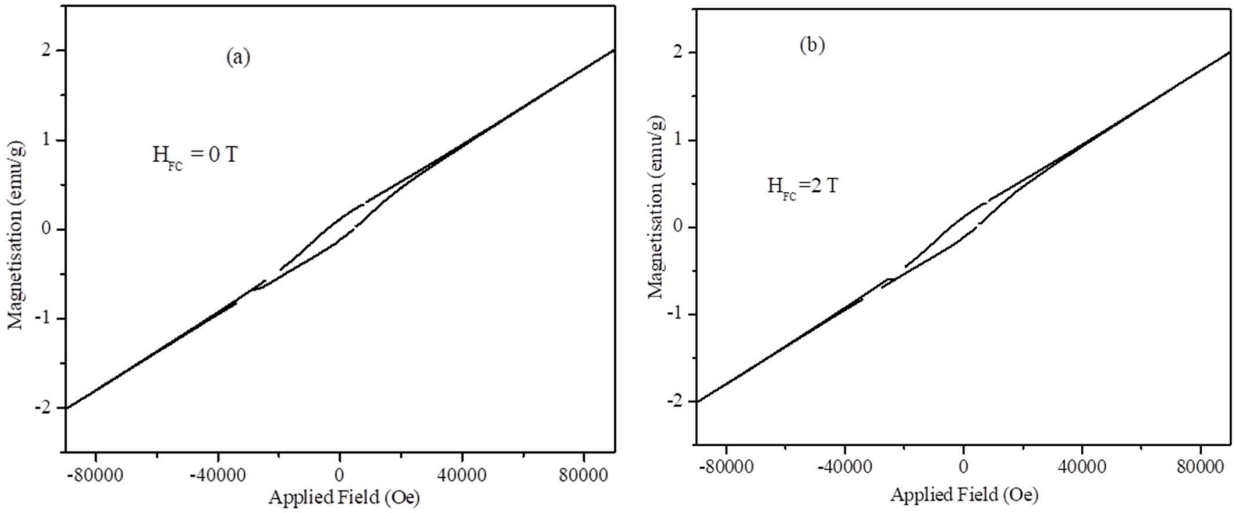

Figure 7. The M-H hysteresis loops at room temperature and sweeping field between −9 and 9 T for (a) the zero-field-cooled state, and (b) the 2 T-field-cooled-state.

It is very important to point out that our calculations of H_{EB}, M_Y and H_C were based on the minor hysteresis loops. It is known that hysteresis loop shifts might occur due to the unsaturated magnetization loops (minor loops) and could lead to misinterpretation of the observation to be due to exchange bias effect [35,36]. However, this is a matter of controversy [37,38]. Nevertheless, it is very important to realize that obtaining hysteresis loop shifts from minor loops does not mean that exchange bias coupling is absent. In some cases, both effects (minor loops and magnetic exchange coupling) coexist and contribute to the loop shifts. In such cases, it is very difficult to isolate the contribution of either one. However, there are some signatures of the exchange coupling that are difficult to understand by considering only the effect of minor loop. As it is known, the magnitude of the minor loop shift depends on the maximum applied field (but smaller than the anisotropy field) reached in the hysteresis measurements. Changing the maximum field will result in different magnitude of loop shift. In some magnetic materials, it will not require large magnetic field to reach saturation magnetization. In antiferromagnetic materials were spin-flopping takes place reaching saturation magnetization requires the application of very large magnetic fields which are usually not available in normal laboratories. However, we believe that the loop shifts appeared in our magnetic measurements are not solely due to the minor hysteresis loops but also due to the magnetic exchange coupling [17]. We also believe that the behavior of the loop shifts as function of temperature and FC values is attributed only to the exchange bias coupling. In all our magnetic hysteresis measurements, the maximum field used was the

same on the ascending and descending branches (−5 and 5 T) at all FC values and for all temperatures. In addition, the experiments were conducted under the same initial conditions. It is seen in Figure 6 that the magnitudes of the H_{EB} in the ZFC state are clearly distinct from those in the FC state at all temperatures below T_M. We believe that this effect is an indication of exchange bias coupling in these samples. On the other hand, the nonmonotonic dependence of H_{EB} on the FC values and on temperature is attributed only to the exchange coupling. These nonmonotonic loop shifts with temperature and FC values indicate that the exchange coupling is due to magnetic exchange interaction across the FM (AFM)/SG interface and between the (FM) maghemite and (AFM) hematite nanoparticles mediated by disordered SG structures. These SG regions, have variable internal spin coupling (with multi-valley energies), and thus will display different response to temperature and to the field cooling leading to the nonmonotonic temperature and field dependence. Additionally, we have separated the FM magnetization component from the total magnetization (by subtracting the high field linear AFM contribution), we have obtained saturated ferromagnetic hysteresis loops that displayed horizontal and vertical loop shifts as shown in Figure 8 (for the zero-field-cooled state at 200, 300 K). Hence, we believe that exchange bias contributed significantly towards the shifted FM loops. Of course, there could be another contribution due to the minor loops of the AFM loops. However, in this work, we focus on the behavior and trend of the exchange bias with temperature and field cooling which is due to real exchange coupling at the FM/SG interface (which resulted in the FM loop shifts).

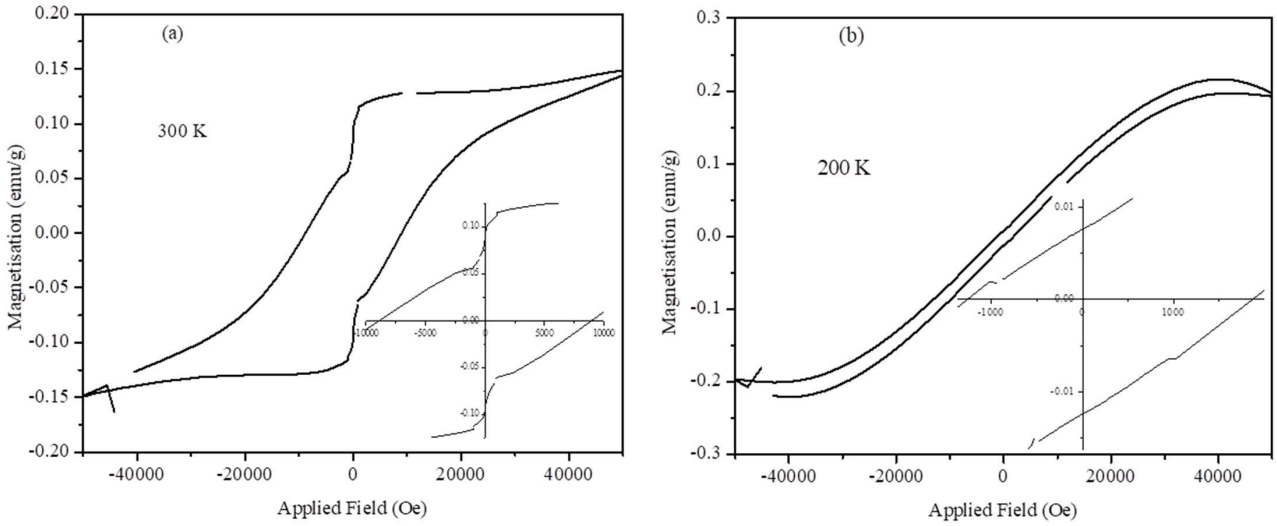

Figure 8. The FM M-H hysteresis loops at the zero-field-cooled state at (a) 300 K and (b) 200 K. The insets show zoomed regions around the origin).

4. Conclusions

The sol-gel method synthesized hematite nanoparticles were characterised by XRD and TEM. A small fraction of maghemite was observed in the XRD spectrum. The M-H plots were obtained by applying a magnetic field in the range of −5 to 5 T. The exchange bias in the ZFC state and in the FC state at various field-cooling values was calculated by measuring the shift in the M-H hysteresis loop

from the origin. Significant H_C, H_{EB} values were observed at room temperature reflecting the significant exchange coupling interaction between the different magnetic phases mediated by SG regions that occur due to canted surface spins. The exchange bias and coercivity in our sample were attributed to the indirect magnetic exchange interaction between the AFM and FM nanoparticles mediated by SG regions.

Acknowledgments

The authors wish to thank University of Sharjah and Sharjah Research Academy for the Collaborative Research Grant #2101050262. The authors also thank the Research Institute of Medical and Health Sciences (RIMHS) at University of Sharjah.

Conflict of interest

All authors declare no conflicts of interest in this paper.

References

1. Colombo M, Carregal S, Casula MF, et al. (2012) Biological applications of magnetic nanoparticles. *Chem Soc Rev* 41: 4306–4334. https://doi.org/10.1039/c2cs15337h
2. Angelakeris M (2017) Magnetic nanoparticles: A multifunctional vehicle for modern theranostics. *BBA Gen Subjects* 1861: 1642–1651. https://doi.org/10.1016/j.bbagen.2017.02.022
3. Issa B, Qadri S, Obaidat IM, et al. (2011) PEG coating reduces NMR relaxivity of $Mn_{0.5}Zn_{0.5}Gd_{0.02}Fe_{1.98}O_4$ hyperthermia nanoparticles. *J Magn Reson Imaging* 34: 1192–1198. https://doi.org/10.1002/jmri.22703
4. Atabaev TS, Vu HHT, Ajmal M, et al. (2015) Dual-mode spectral convertors as a simple approach for the enhancement of hematite's solar water splitting efficiency. *Appl Phys A-Mater* 119: 1373–1377. https://doi.org/10.1007/s00339-015-9108-1
5. Boutchuen A, Zimmerman D, Aich N, et al. (2019) Increased plant growth with hematite nanoparticle fertilizer drop and determining nanoparticle uptake in plants using multimodal approach. *J Nanomater* 2019: e6890572. https://doi.org/10.1155/2019/6890572
6. Obaidat IM, Mohite V, Issa B, et al. (2009) Predicting a major role of surface spins in the magnetic properties of ferrite nanoparticles. *Cryst Res Technol* 44: 489–494. https://doi.org/10.1002/crat.200900022
7. Obaidat IM, Issa B, Haik Y (2011) The role of aggregation of ferrite nanoparticles on their magnetic properties. *J Nanosci Nanotechnol* 11: 3882–3888. https://doi.org/10.1166/jnn.2011.3833
8. Bañobre LM, Teijeiro A, Rivas J (2013) Magnetic nanoparticle-based hyperthermia for cancer treatment. *Rep Pract Oncol Radiother* 18: 397–400. https://doi.org/10.1016/j.rpor.2013.09.011
9. Laurent S, Elst LV, Muller RN (2013) Superparamagnetic iron oxide nanoparticles for MRI, In: *The Chemistry of Contrast Agents in Medical Magnetic Resonance Imaging*, 2 Eds., New York: John Wiley & Sons, 427–447. https://doi.org/10.1002/9781118503652.ch10

10. Cornell RM, Schwertmann U (2003) *The Iron Oxides: Structure, Properties, Reactions, Occurrences and Uses*, 2 Eds., New York: John Wiley & Sons. https://doi.org/10.1002/3527602097
11. Demortière A, Panissod P, Pichon BP, et al. (2011) Size-dependent properties of magnetic iron oxide nanocrystals. *Nanoscale* 3: 225–232. https://doi.org/10.1039/C0NR00521E
12. Ashraf M, Khan I, Usman M, et al. (2020) Hematite and magnetite nanostructures for green and sustainable energy harnessing and environmental pollution control: a review. *Chem Res Toxicol* 33: 1292–1311. https://doi.org/10.1021/acs.chemrestox.9b00308
13. Xue Y, Wang Y (2020) A review of the α-Fe_2O_3 (hematite) nanotube structure: recent advances in synthesis, characterization, and applications. *Nanoscale* 12: 10912–10932. https://doi.org/10.1039/D0NR02705G
14. Liu J, Yang H, Xue X (2019) Preparation of different shaped α-Fe_2O_3 nanoparticles with large particles of iron oxide red. *CrystEngComm* 21: 1097–1101. https://doi.org/10.1039/C8CE01920G
15. Stewart S, Borzi R, Cabanillas E, et al. (2003) Effects of milling-induced disorder on the lattice parameters and magnetic properties of hematite. *J Magn Magn Mater* 260: 447–454. https://doi.org/10.1016/S0304-8853(02)01388-4
16. Muench GJ, Arajs S, Matijević E (1985) The morin transition in small α-Fe_2O_3 particles. *Phys Status Solidi A* 92: 187–192. https://doi.org/10.1002/pssa.2210920117
17. Bhowmik RN, Saravanan A (2010) Surface magnetism, morin transition, and magnetic dynamics in antiferromagnetic α-Fe_2O_3 (hematite) nanograins. *J Appl Phys* 107: 053916. https://doi.org/10.1063/1.3327433
18. Lee JB, Kim HJ, Lužnik J, et al. (2014) Synthesis and magnetic properties of hematite particles in a "Nanomedusa" morphology. *J Nanomater* 2014: e902968. https://doi.org/10.1155/2014/902968
19. Shimomura N, Pati SP, Sato Y, et al. (2015) Morin transition temperature in (0001)-oriented α-Fe_2O_3 thin film and effect of Ir doping. *J Appl Phys* 117: 17C736. https://doi.org/10.1063/1.4916304
20. Hansen MF, Koch CB, Lefmann K, et al. (2000) Magnetic properties of hematite nanoparticles. *Phys Rev B* 61: 6826–6838. https://doi.org/10.1103/PhysRevB.61.6826
21. Suber L, Santiago AG, Fiorani D, et al. (1998) Structural and magnetic properties of α-Fe_2O_3 nanoparticles. *Appl Organomet Chem* 12: 347–351. https://doi.org/10.1002/(SICI)1099-0739(199805)12:5%3C347::AID-AOC729%3E3.0.CO;2-G
22. Ihab MO, Sulaiman A, Imad AAO, et al. (2020) Field-dependent morin transition and temperature-dependent spin-flop in synthetic hematite nanoparticles. *Curr Nanosci* 16: 967–975. https://doi.org/10.2174/1573413716666191223124722
23. Nogués J, Sort J, Langlais V, et al. (2005) Exchange bias in nanostructures. *Phys Rep* 422: 65–117. https://doi.org/10.1016/j.physrep.2005.08.004
24. Obaidat IM, Nayek C, Manna K, et al. (2017) Investigating exchange bias and coercivity in Fe_3O_4-γ-Fe_2O_3 core-shell nanoparticles of fixed core diameter and variable shell thicknesses. *Nanomaterials* 7: 415. https://doi.org/10.3390/nano7120415
25. Rui WB, Hu Y, Du A, et al. (2015) Cooling field and temperature dependent exchange bias in spin glass/ferromagnet bilayers. *Sci Rep* 5: 13640. https://doi.org/10.1038/srep13640

26. Hajra P, Basu S, Dutta S, et al. (2009) Exchange bias in ferrimagnetic-antiferromagnetic nanocomposite produced by mechanical attrition. *J Magn Magn Mater* 321: 2269–2275. https://doi.org/10.1016/j.jmmm.2009.01.037
27. Fiorani D, Del Bianco L, Testa AM (2006) Glassy dynamics in an exchange bias nanogranular system: Fe/FeO_x. *J Magn Magn Mater* 300: 179–184. https://doi.org/10.1016/j.jmmm.2005.10.059
28. Desautels RD, Skoropata E, Chen YY, et al. (2011) Tuning the surface magnetism of γ-Fe_2O_3 nanoparticles with a Cu shell. *Appl Phys Lett* 99: 262501. https://doi.org/10.1063/1.3671989
29. Nogués J, Schuller IK (1999) Exchange bias. *J Magn Magn Mater* 192: 203–232. https://doi.org/10.1016/S0304-8853(98)00266-2
30. Berkowitz AE, Takano K (1999) Exchange anisotropy–a review. *J Magn Magn Mater* 200: 552–570. https://doi.org/10.1016/S0304-8853(99)00453-9
31. Giri S, Patra M, Majumdar S (2011) Exchange bias effect in alloys and compounds. *J Phys Condens Matter* 23: 073201. https://doi.org/10.1088/0953-8984/23/7/073201
32. Goswami S, Bhattacharya D, Roy S, et al. (2013) Superspin glass mediated giant spontaneous exchange bias in a nanocomposite of $BiFeO_3$. *Phys Rev Lett* 110: 107201. https://doi.org/10.1103/PhysRevLett.110.107201
33. Ali M, Adie P, Marrows CH (2007) Exchange bias using a spin glass. *Nat Mater* 6: 70–75. https://doi.org/10.1038/nmat1809
34. Liu Y, Ren P, Xia B, et al. (2011) Large exchange bias after zero-field cooling from an unmagnetized state. *Phys Rev Lett* 106: 077203. https://doi.org/10.1103/PhysRevLett.106.077203
35. Greenwood NN, Greatrex R (1971) High-spin iron complexes, *Mössbauer Spectroscopy*, Netherlands: Springer, 112–168. https://doi.org/10.1007/978-94-009-5697-1_6
36. Harres A, Mikhov M, Skumryev V, et al. (2016) Criteria for saturated magnetization loop. *J Magn Magn Mater* 402: 76–82. https://doi.org/10.1016/j.jmmm.2015.11.046
37. Luo W, Wang F (2007) Cluster glass induced exchange biaslike effect in the perovskite cobaltites. *Phys Rev Lett* 90: 162515. https://doi.org/10.1063/1.2730737
38. Fita I, Wisniewski A, Puzniak R, et al. (2008) Surface and exchange-bias effects in compacted $CaMnO_3$ nanoparticles. *Phys Rev B* 77: 054410. https://doi.org/10.1103/PhysRevB.77.054410

AIMS Press